Aerodynamic Performance of the Low-Earth Orbit Flight Test of an Inflatable Decelerator (LOFTID) Technology Demonstration Mission

Ashley M. Korzun*, Brian R. Hollis†, Adam J. Wise‡, and Derek S. Liechty§
NASA Langley Research Center, Hampton, VA, 23666, USA

Christopher D. Karlgaard¶ and Rohan G. Deshmukh‖
Analytical Mechanics Associates, Inc., Hampton, VA, 23666, USA

The Low-Earth Orbit Flight Test of an Inflatable Decelerator (LOFTID) mission successfully demonstrated the deployment and entry performance of a 6 m diameter Hypersonic Inflatable Decelerator on November 10, 2022. This was the largest blunt body flown to date and demonstrated this inflatable aeroshell technology at scale and conditions relevant to Earth and Mars Entry, Descent, and Landing applications. LOFTID built upon the prior successes of the suborbital IRVE and IRVE-3 missions, leveraging and expanding on the flight experience from these and other planetary and Earth sample return missions. Both the re-entry vehicle and ejectable data module were successfully recovered from the Pacific Ocean, with LOFTID satisfying requirements for decelerator performance and stable flight from orbital entry conditions through parachute deployment and splashdown. This work discusses the pre-flight aerodynamics database and reconstructed flight performance of the LOFTID re-entry vehicle.

Nomenclature

C_A	axial force coefficient
C_l	rolling moment coefficient
C_m	pitching moment coefficient
C_{m_q}	pitch damping coefficient
C_N	normal force coefficient
C_n	yawing moment coefficient
C_{n_r}	yaw damping coefficient
C_Y	side force coefficient
D	capsule diameter, m
Kn	Knudsen number
M	Mach number
q	Dynamic pressure, Pa
U	Uncertainty
V	atmosphere-relative velocity, m/s
X, Y, Z	capsule coordinates from nose, m
α	angle of attack, deg
β	angle of sideslip, deg
γ	inertial flight path angle, deg
σ	standard deviation

Superscripts and Subscripts

A	adder
C	coefficient
CG	center of gravity
$disp$	dispersed quantity
M	multiplier
T	total condition
∞	freestream condition

I. Introduction

On November 10, 2022, the Low-earth Orbit Flight Test of an Inflatable Decelerator (LOFTID) successfully demonstrated the stable flight and system performance of a Hypersonic Inflatable Aerodynamic Decelerator (HIAD)

*Senior Technical Lead, Atmospheric Flight and Entry Systems Branch, M/S 489, and AIAA Associate Fellow.
†Senior Technical Lead, Aerothermodynamics Branch, and AIAA Associate Fellow.
‡Aerospace Engineer, Aerothermodynamics Branch, AIAA Member.
§Aerospace Engineer, Aerothermodynamics Branch, AIAA Member.
¶Aerospace Engineer, Atmospheric Flight and Entry Systems Branch, AIAA Associate Fellow.
‖Aerospace Engineer, Atmospheric Flight and Entry Systems Branch, AIAA Member.

[1]. This technology demonstration mission launched as a secondary payload with the Joint Polar Satellite System-2 (JPSS-2) weather satellite on a United Launch Alliance Atlas V launch vehicle from Vandenberg Space Force Base along the coast of California. With a 6 m diameter, this was the largest blunt body aeroshell ever flown and demonstrated HIAD technology at scale and conditions relevant to Earth and Mars Entry, Descent, and Landing (EDL) applications. A HIAD is a deployable, inflatable aeroshell that functions as both a heatshield and as a decelerator. Whereas rigid aeroshells are limited to the diameter of a launch vehicle fairing, a deployable aeroshell such as a HIAD can be stowed and then deployed to a much larger diameter, and subsequently drag area, than would otherwise fit within a payload fairing. HIADs have a number of applications, including low-Earth orbit return, International Space Station down-mass, delivery of significantly larger payloads to the surface of Mars, and launch vehicle asset recovery at Earth. LOFTID built upon the prior success of the Inflatable Re-entry Vehicle Experiments (IRVE [2] and IRVE-3 [3]), which were suborbital flights of 3 m diameter HIADs, through a technology demonstration mission with a 6 m diameter HIAD completing entry from low-Earth orbit conditions.

Figure 1 shows the IRVE-3 and LOFTID re-entry vehicles, and Table 1 summarizes key differences between the two vehicles and missions. Compared to IRVE-3, LOFTID experienced nearly three times the entry velocity and more than double the peak heat rate. IRVE and IRVE-3 were 60° sphere-cone geometries, sharper in both cone angle and nose radius than LOFTID. Increasing the cone half-angle from 60° to 70° for LOFTID permitted a larger diameter HIAD for a given mass, packed volume, and inflation volume. This change represented a worse case for demonstrating the capabilities of the inflatable structure under drag loading, represented a more challenging case for dynamic stability and drag loading for the inflatable structure, while providing a Mars-like heating environment.

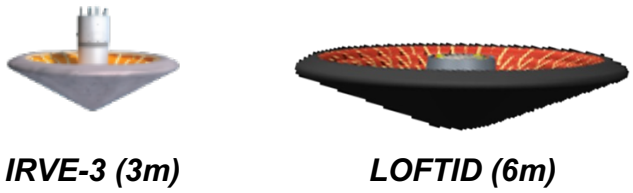

Fig. 1 HIAD Re-entry Vehicles: IRVE-3 and LOFTID.

Table 1 Comparison Between HIAD Re-entry Vehicles

	IRVE-3	LOFTID
HIAD Maximum Diameter (m)	3.0	6.0
Forebody Cone Half-Angle	60°	70°
Entry Mass (kg)	330	1100
Entry Velocity (km/s)	2.7	8.0
Peak Heat Rate (W/cm^2)	15.0	39.8

Figure 2 shows the concept of operations for LOFTID. Following launch into orbit and separation of the primary payload, the LOFTID aeroshell, or Re-entry Vehicle (RV) was inflated, oriented for entry, spun up to 18 deg/s, and separated from the Centaur upper stage of the launch vehicle. The mission officially ended when the RV reached Mach 0.7 and the ejectable data module (EDM) jettisoned for recovery. Deceleration of the RV continued through subsonic conditions with the eventual deployment of a parachute and splashdown in the Pacific Ocean off the coast of Hawaii. While not a requirement, it was highly desirable to recover the RV, and both the EDM and the RV were successfully recovered from the ocean post flight.

The total time of flight from RV separation to splashdown was just under 56 minutes (3356.44 s). At atmospheric interface (125 km altitude), the RV was traveling at 7.95 km/s with with a shallow entry flight path angle (γ) of -2.29°. Peak heating occurred at Mach 25.39 (39.77 W/cm^2). Peak deceleration occurred at Mach 14.27 (8.98 Earth g's), and peak dynamic pressure occurred at Mach 13.93 (2.08 kPa). LOFTID demonstrated stable flight behavior and successful deceleration from nearly 8 km/s entry velocity with a blunt-body, inflatable aeroshell, flying a spin-stabilized, unguided,

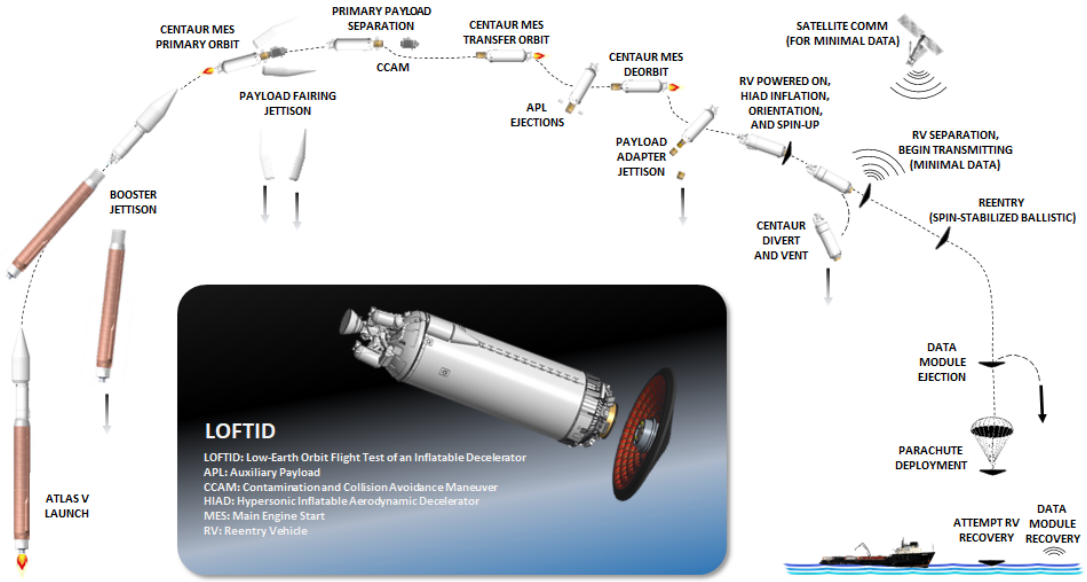

Fig. 2 LOFTID Concept of Operations.

ballistic trajectory. The RV was instrumented with an Inertial Measurement Unit (IMU) and Flush Air Data Sensing (FADS) system to provide data for post-flight reconstruction, as well as on-board video. The IMU data were not captured by the data recorder due to a malfunction [4], and the reconstruction of the atmospheric-relative trajectory and attitude was subsequently completed using the FADS system and on-board video data through photogrammetry [4, 5]. Complete details on the trajectory and atmosphere reconstruction are provided by Karlgaard et al. [5], and the flight mechanics analysis is further discussed by Deshmukh et al. [6].

The remainder of this paper is organized as follows: Section II describes the pre-flight aerodynamics database (ADB) and dispersions used to quantify flight performance of the LOFTID RV in its deployed configuration from entry interface through splashdown. Section III discusses the as-flown aerodynamic performance and contributing factors to the departures from pre-flight performance predictions in the context of aerodynamics.

II. Pre-Flight Aerodynamics Predictions

Aerodynamic forces and moments are key contributors to entry vehicle performance, including drag and stability. The LOFTID mission was required to produce the equivalent hypersonic aerodynamic drag of a rigid aeroshell of the same geometry and to maintain a total angle of attack less than 20° from entry through Mach 0.7 conditions (stable flight). This section describes the development and implementation of the aerodynamics database used to support design and pre-flight performance assessments for LOFTID.

A. Vehicle Geometry and Reference Trajectory

LOFTID's 70° sphere-cone geometry was constructed from an inflatable structure and flexible thermal protection system, which when fully deployed and inflated, functioned as both a decelerator and heatshield. Drawing direct heritage from the 3 m diameter HIADs flown previously on IRVE [2] and IRVE-3 [3], this 6 m diameter aeroshell, shown in Fig. 3, was the largest blunt body aeroshell flown to date, rigid or deployable. There was no backshell; the payload was fully exposed. Figure 3 also defines the aerodynamics coordinate frame, typical for blunt-body entry shapes. The geometry of the RV was modeled to be fully smooth, rigid, and axisymmetric for the purpose of aerodynamic analyses.

To demonstrate satisfaction of mission requirements, the aerodynamics database was developed to cover the entire trajectory from atmospheric interface (125 km altitude) to splashdown and span the range of potential conditions and attitudes anticipated in flight across design maturation of the RV, atmosphere variability, and launch window impacts. The ADB developed for LOFTID provides six degree-of-freedom (DOF) aerodynamic force and moment coefficients as a model input to the trajectory simulation as a function of flight conditions and vehicle attitude. The model spans

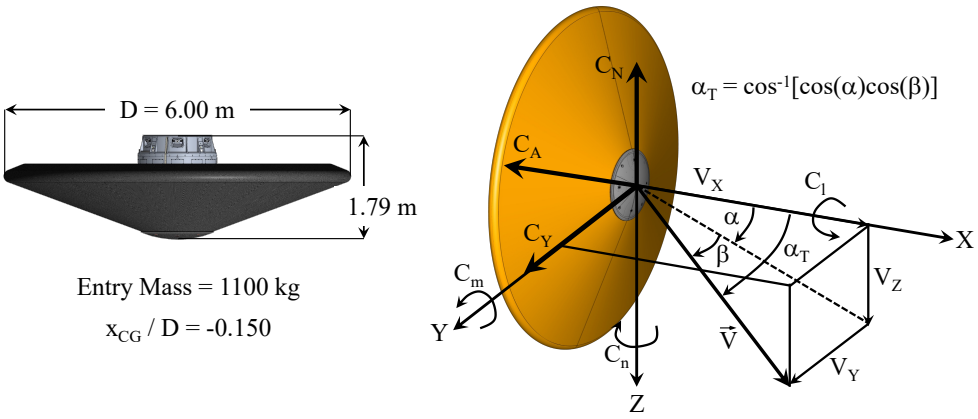

Fig. 3 LOFTID Geometry (left) and Aerodynamics Coordinate Frame (right).

non-continuum and continuum flight regimes, static aerodynamics and dynamic pitch damping, and uncertainties as a function of flight regime. Inputs to the aerodynamics database are freestream Knudsen number (Kn), Mach number (M_∞), angle of attack (α), and angle of sideslip (β). Aerodynamic force and moment coefficients are specified by total angle of attack (α_T) with the assumption that the RV is axisymmetric and through logic to use data for the appropriate flight regime (free-molecular, transitional, hypersonic, supersonic, transonic, and subsonic). Dispersion of aerodynamic coefficients for Monte Carlo trajectory analysis are also handled within the aerodynamics database, and details on the implementation are given in Section II.D.

The aerodynamics datasets, methods, tools, and implementation draw strongly on heritage from IRVE [7], IRVE-3 [3], and other NASA entry capsule missions [8–10]. Different computational tools and methods are required for each flow regime to capture relevant physics, and these tools, methods, heritage, and applicability are briefly discussed in the following sections, with further details provided in Ref. [11]. Figure 4 shows the design reference trajectory as a function of both time and velocity, with flow regimes noted and the static anchor points from the aerodynamics database denoted along the reference trajectory. Individual conditions are simulated using more than one computational approach across the boundaries of each flow regime (indicated by the overlap conditions in Fig. 4b) and the data blended through the transition. The following sections describe the static aerodynamics, dynamic pitch damping, and uncertainties developed and applied for LOFTID.

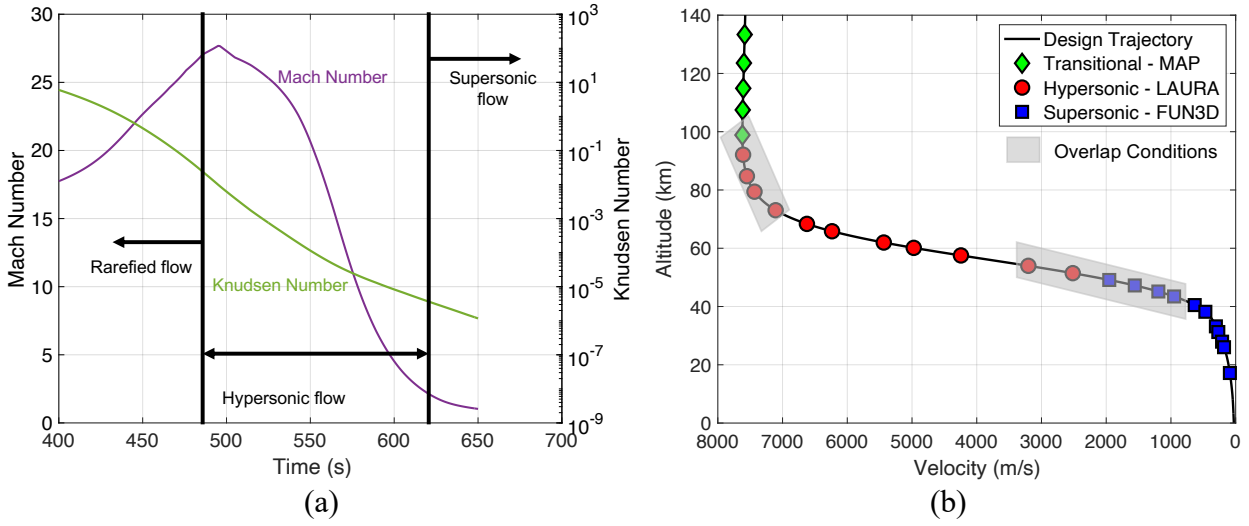

Fig. 4 LOFTID Reference Trajectory (a) and Aerodynamics Database Anchor Points (b).

B. Static Aerodynamics

The tools and methods applied to generate static aerodynamics data for LOFTID have been successfully applied to and validated by flight at both Earth and Mars for blunt entry capsules with strong detached shocks and highly separated wake flows. Table 2 outlines the organization of the ADB by flight regime, including the range of conditions, input parameters, and data source. All static aerodynamics data for LOFTID are sourced from computational tools, sharing solutions generated for aerothermodynamics analysis [11]. The assumption that the vehicle is axisymmetric allows the aerodynamic coefficients to be defined in the α_T plane and then decomposed into the α and β planes for use in the 6-DOF trajectory simulation (see Fig. 3).

Table 2 LOFTID Static Aerodynamics Sources

	Flight Regime	Range	Input Parameters	Source
Non-Continuum	Free-Molecular	$Kn > 3.018$, $0^\circ \leq \alpha_T \leq 180^\circ$	α_T	DAC [12]
	Transitional	$0.00572 \leq Kn \leq 3.018$, $0^\circ \leq \alpha_T \leq 8^\circ$	α_T, Kn	MAP [13]
Continuum	Hypersonic	$M_\infty \geq 7.88$ and $Kn < 0.00572$, $0^\circ \leq \alpha_T \leq 8^\circ$	α_T, M_∞	LAURA [14]
	Supersonic	$0.89 < M_\infty \leq 6.10$, $0^\circ \leq \alpha_T \leq 20^\circ$	α_T, M_∞	FUN3D [15]
	Mid-Subsonic	$0.30 < M_\infty \leq 0.89$, $0^\circ \leq \alpha_T \leq 40^\circ$	α_T, M_∞	FUN3D
	Low-Subsonic	$M_\infty \leq 0.30$, $0^\circ \leq \alpha_T \leq 40^\circ$	α_T	FUN3D

At the highest altitude conditions below the atmospheric interface (125 km), non-continuum aerodynamics require prediction using methods that account for molecular interactions between individual molecules and those molecules with the vehicle. Due to the similarity in general shape and high-altitude environment, free-molecular data originally generated for IRVE-3 [3] using the Direct Simulation Monte Carlo (DSMC) Analysis Code (DAC [12]) were used for conditions where $Kn > 3.018$ (above 133 km on the design reference trajectory) and tabulated for α_T from 0° to 180°. Transitional data were generated using the MAP [13] DSMC code to populate additional low-density conditions down to $Kn = 0.00572$ (92 km) and directly bridge the free-molecular and continuum flow regimes [11]. The transitional flow data were generated for α_T from 0° to 8°, with the α_T range guided by permissible RV separation conditions and the ballistic trajectory design. These flow solutions employed reacting gas chemistry with surface catalysis and Cartesian/cut-cell grid topologies; the top section of Fig. 5 shows an example MAP solution for LOFTID at a non-zero angle of attack. Hypersonic continuum data were generated using the LAURA Navier-Stokes flow solver [11, 14, 16] with non-equilibrium chemistry and structured grid topologies. The middle of Fig. 5 shows an example LAURA mesh and flow solution, with forebody-only data used within the ADB for this flight regime. Hypersonic continuum data in the ADB span Mach numbers from 27.2 to 6.1 and total angles of attack from 0° to 8°, with the α_T range intended to bound any potential excursions from the ballistic trajectory design due to small unintended changes in shape or mass properties.

The remaining static aerodynamics along the design reference trajectory were generated using the FUN3D Navier-Stokes flow solver [11, 15], with an example mesh and solution shown at the bottom of Fig. 5. For supersonic, transonic, and subsonic conditions, data were generated for Mach numbers from 6.1 down to 0.3 and a wider range of α_T (0° to 40°) to avoid potential extrapolation through conditions where blunt body geometries characteristically exhibit attitude growth due to inherent dynamic instability at low supersonic Mach numbers. Supersonic static coefficients in many prior ADBs [8–10, 17] used forebody computational fluid dynamics (CFD) solutions with a Viking-derived pressure correction for aftbody contributions [9, 17], but these shapes all have full backshells protruding into the wake. For supersonic and subsonic conditions, IRVE and IRVE-3 used static coefficients derived from ballistic range testing [2, 3], as the aft configurations, like LOFTID, lacked a backshell and instead had a predominantly concave geometry with a slender, protruding payload along the center axis. LOFTID used time-averaged, unsteady Navier-Stokes three-dimensional flow solutions from FUN3D, including the aft payload geometry and wake, perfect-gas air assumptions, and fully unstructured grids, for all conditions in the ADB from Mach 6.1 to 0.3. These data were used for the RV while descending under parachute through to splashdown, with static aerodynamics coefficients for all conditions below Mach 0.3 held constant at the Mach 0.3 values, though still a function of α_T.

Figures 6, 7, and 8 show the nominal static aerodynamics for axial force coefficient and pitching moment coefficient, where C_m is shown about the center-of-gravity (CG) location 0.150 diameters aft of the nose. Axial force dominates the aerodynamic forces on blunt body vehicles ($C_A >> C_N$). As the vehicle decelerates from the top of the atmosphere, C_A

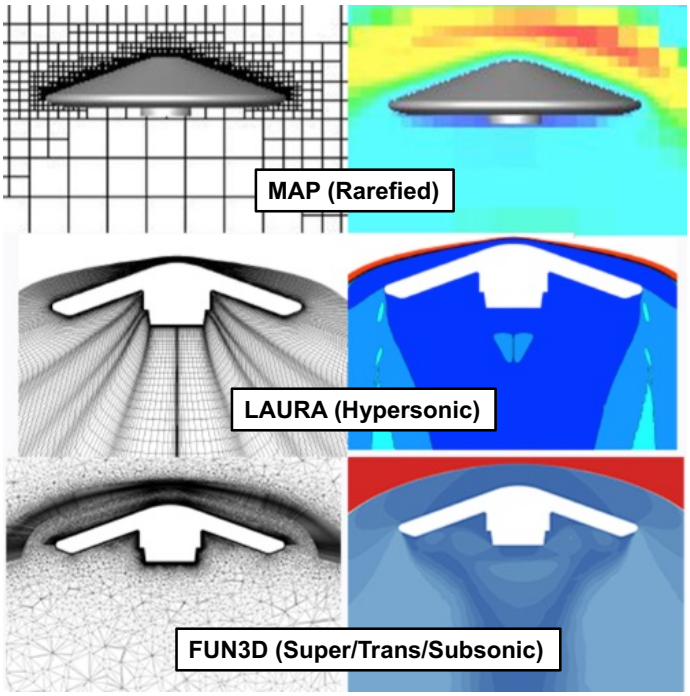

Fig. 5 Examples of Mesh and Flow Solutions for Computationally Modeled Static Aerodynamics Data.

continuously decreases from rarefied to continuum conditions. C_A is greatest at the lowest angles of attack, consistent with the forebody surfaces being by far the most significant contributor to the pressure load on the vehicle. C_A continues to gradually decrease as the vehicle decelerates further, until reaching low-supersonic conditions. Beginning near Mach 3.0, C_A rises with decreasing Mach number, as the pressure on the aft surfaces of the vehicle contributes a non-negligible pressure increment to the overall axial force. The aft pressure effects are less sensitive to angle of attack, and as the vehicle decelerates further, the strong pressure recovery across the shock disappears, and C_A quickly falls to a minimum. For conditions below Mach 0.3, C_A is held constant at the incompressible Mach 0.3 value and is then only a function of α_T.

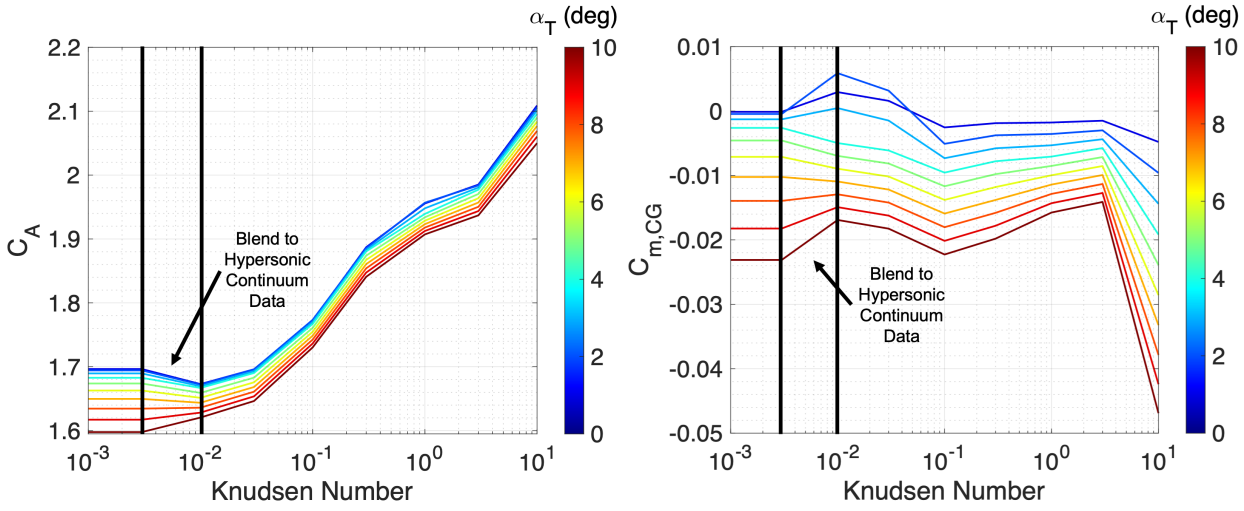

Fig. 6 LOFTID Non-Continuum Static Aerodynamics for Axial Force Coefficient (left) and Pitching Moment Coefficient (right).

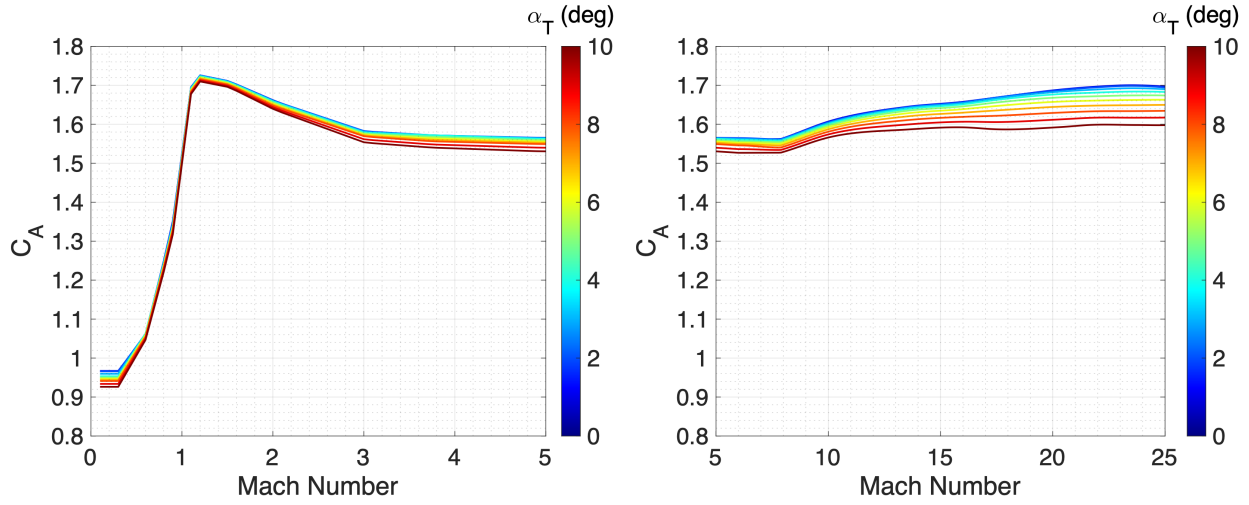

Fig. 7 LOFTID Continuum Axial Force Coefficient Database.

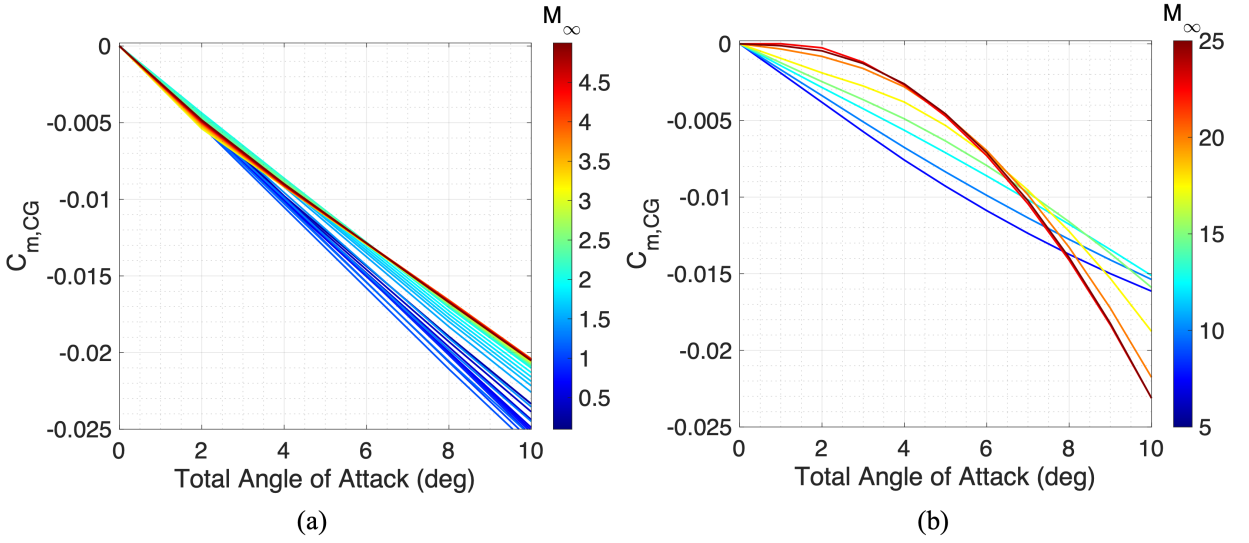

Fig. 8 LOFTID Continuum Pitching Moment Coefficient Database for (a) $M_\infty \leq 5$ and (b) $5 \leq M_\infty \leq 25$.

Figure 8 shows the pitching moment coefficient database for continuum conditions, with C_m plotted about the CG as a function of α_T and M_∞. The vehicle was predicted to be statically stable throughout the continuum conditions along the entry trajectory, as indicated by the persistent negative slope of $C_{m,CG}$ vs. α in Fig. 8. While Fig. 6 shows a small static instability at very low α_T (less than 2°) for $0.01 < Kn < 0.1$, the dynamic pressure at these conditions, due to the very low density at high altitude, produces a near-negligible effect on RV stability.

C. Dynamic Pitch Damping

Blunt body shapes are characteristically dynamically unstable at supersonic speeds [18], with undamped pitch oscillations corresponding to vehicle attitude and attitude rate growth as the vehicle decelerates through supersonic to transonic conditions. These effects have the potential to produce unfavorable dynamics, and for LOFTID, there was a stability requirement for the total angle of attack to not exceed 20° down to Mach 0.7. This allowed for successful deployment of the ejectable data module and later deployment of a subsonic parachute to limit the vertical speed at splashdown to below 6.7 m/s (15 mph). LOFTID deployed a parachute at low subsonic conditions to reduce vertical speed for splashdown, long past where the shape's inherent pitch damping instability is a dominant factor in the vehicle's

dynamics.

Figure 9 shows the LOFTID dynamic pitch damping database. The pitch damping coefficient model is a functional form based on instantaneous angle of attack and Mach number and is derived from ballistic range testing conducted for IRVE-3 [3]. The variable C_{m_q} here is the sum $C_{m_q} + C_{m_{\dot{\alpha}}}$, truncated for brevity. For free-molecular conditions, the vehicle is assumed to be dynamically stable at a fixed value of C_{m_q} = -0.32. For continuum conditions above Mach 6, the vehicle is dynamically stable ($C_{m_q} < 0$), with C_{m_q} fixed at a value estimated from Newtonian flow approximations. Between free-molecular and hypersonic continuum conditions, the value of C_{m_q} is computed as a function of Kn using a sine-squared bridging function. The vehicle is dynamically unstable ($C_{m_q} > 0$), for $M_\infty < 3.5$ at very small angles of attack. For $M_\infty < 2.0$, the vehicle is dynamically unstable, but for a slightly larger range of angle of attack, up to 5°. For $M_\infty < 0.65$, C_{m_q} is held constant at the $M_\infty = 0.65$ value.

Table 3 LOFTID Dynamic Pitch Damping Sources

	Flight Regime	Range	Input Parameters	Source
Non-Continuum	Free-Molecular	$Kn \geq 10.0$, $0° \leq \alpha_T \leq 180°$	none	–
	Transitional	$0.001 < Kn < 10.0$, $0° < \alpha_T < 40°$	α_T, Kn	–
Continuum	Hypersonic	$M_\infty \geq 6.0$ and $Kn < 0.001$, $0° \leq \alpha_T \leq 40°$	α_T, M_∞	IRVE-3
	Supersonic	$0.65 \leq M_\infty < 3.0$, $0° \leq \alpha_T \leq 40°$	α_T, M_∞	IRVE-3
	Subsonic	$M_\infty < 0.65$, $0° \leq \alpha_T \leq 40°$	α_T, M_∞	IRVE-3

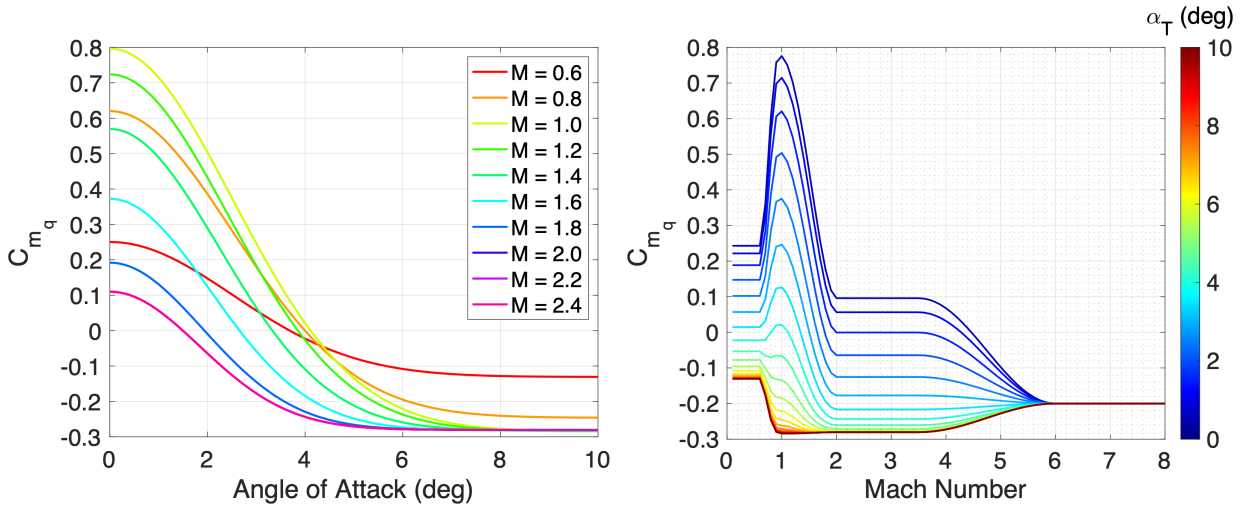

Fig. 9 LOFTID Dynamic Damping Database.

D. Aerodynamics Uncertainties

Pre-flight performance for LOFTID was assessed using Monte Carlo simulations with 6-DOF trajectories in the Program to Optimize Simulated Trajectories II (POST2) [6]. Uncertainties on the nominal aerodynamics data were defined within the ADB to allow for dispersion of aerodynamics within the analyses, with significant heritage from past flight experience and engineering judgement from IRVE, IRVE-3, Genesis, and Phoenix. Table 4 lists the aerodynamics uncertainties applied for LOFTID. Similar to the structure of the ADB for nominal aerodynamics, the uncertainties were defined by relevant flow regime. The differences in uncertainty magnitudes in Table 4 reflect differences in applicability, fidelity, and uncertainty in the underlying tools, methods, and sources used to generate the nominal aerodynamic coefficients. For all static coefficients other than C_A, uncertainty adders and multipliers were applied to independently disperse trim attitude (intercept) and static stability (slope), respectively. Eq. 1 specifies the implementation of the static aerodynamics adders and multipliers given in Table 4. Uncertainties were applied after the ADB coefficients have been

decomposed into the vehicle body frame (see Fig. 3), and all moments were dispersed about the CG, not the moment reference point (center of the heatshield).

Table 4 LOFTID aerodynamics uncertainties

Static Aerodynamics (Uncorrelated)

Flight Regime	C_A	C_N, C_Y	C_m, C_n	C_l
Free-Molecular / Transitional $Kn > 0.1$	±5%	±0.01, ±20%	±0.005, ±20%	$\pm 1.24 \times 10^{-6}$
Hypersonic $M_\infty < 10$	±3%	±0.01, ±20%	±0.003, ±20%	$\pm 1.24 \times 10^{-6}$
Supersonic $1.5 < M_\infty < 5$	±10%	±0.01, ±20%	±0.005, ±20%	$\pm 1.24 \times 10^{-6}$
Transonic $0.4 < M_\infty < 1.5$	±10%	1.25 × Supersonic	1.25 × Supersonic	$\pm 1.24 \times 10^{-6}$

Dynamic Damping (Correlated)

Flight Regime	C_{m_q}	C_{n_r}
Transitional / Free-Molecular $Kn > 0.1$	±0.15	±0.15
Hypersonic $M_\infty > 6$	±0.15	±0.15
Supersonic $1.5 < M_\infty < 3$	$+0.4 \times [1.5, 0.5] - 0.4 + [0.1, 0.0]$	$+0.4 \times [1.5, 0.5] - 0.4 + [0.1, 0.0]$
Transonic $1 < M_\infty < 1.5$	1.25 × Supersonic	1.25 × Supersonic

All static aerodynamics uncertainties were uncorrelated and dispersed using a normal distribution, with the exception of C_l, which was dispersed using a uniform distribution. Increases in the multipliers for C_Y and C_N were applied over the IRVE-3 uncertainties as a result of potential limited deflection of the inflatable aeroshell under load. The uncertainty in C_{m_q} was fixed to be equal to that in C_{n_r}, and the implementation is specified in Eqn. 2. For dynamic aerodynamics uncertainties, at hypersonic conditions, uncertainties were applied assuming a uniform distribution, and at supersonic and transonic conditions, the uncertainty adder was applied assuming a uniform distribution, and the uncertainty multiplier was applied assuming a normal distribution. An additional shift was applied to force a larger portion of the Monte Carlo cases to be less dynamically stable. The shift magnitude of 0.4 for $M_\infty < 3.0$ bounded the ballistic range data underpinning the dynamic pitch damping model.

$$C_{disp} = [C_{nominal}(\alpha, \beta) + U_C^A](1 + U_C^M) \tag{1}$$

$$C_{m_q,disp} = (C_{m_q,nominal}(\alpha, \beta) - 0.4) * U_C^M + 0.4 + U_C^A \tag{2}$$

III. LOFTID As-Flown Aerodynamic Performance

The LOFTID RV was instrumented to provide data for post-flight assessment of vehicle performance and verification of mission requirements. As mentioned in Section I, the IMU data were not captured by the data recorder due to a malfunction [4], and the reconstruction of the atmospheric-relative trajectory and attitude was possible using the FADS and on-board video data through photogrammetry [4, 5]. Complete details on the instrumentation, trajectory analysis,

and post-flight reconstruction are provided by Swanson et al. [4], Deshmukh et al. [6], and Karlgaard et al. [5]. The lack of IMU data severely impaired the reconstruction process. Without the IMU data it was not possible to reconstruct the as-flown aerodynamics of the vehicle. Nominal aerodynamics (taken from the ADB) were assumed in order to compute metrics such as loads, which ordinarily would have been directly measured by the IMU.

The FADS data were successfully used to reconstruct the attitude history, as illustrated by Fig. 10. Using estimates from an atmosphere-relative trajectory [5], the total angle of attack history with the dynamic pressure pulse demonstrate success in meeting the LOFTID requirement for RV aerodynamic stability throughout the trajectory, with the total angle of attack remaining below 7° prior to peak dynamic pressure and remaining well below the 20° requirement afterwards. Prior to peak dynamic pressure, the total angle of attack increases from approximately 1.23° at 125 km (atmospheric interface) to a maximum of 6.52°, then sharply drops to less than 1° with increasing dynamic pressure as the aeroshell shifted position slightly from its zero-g inflation location into its nominal drag location relative to the rigid nose. The RV remained at low total angle of attack past peak dynamic pressure until decelerating to approximately Mach 2 conditions. The peak α_T across the entire reconstructed trajectory was 10.41°.

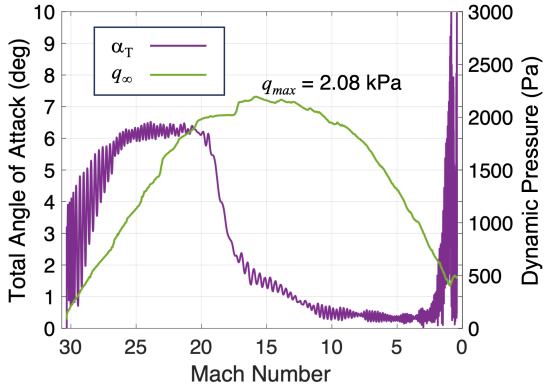

Fig. 10 Reconstructed Total Angle of Attack and Dynamic Pressure.

Figure 11 shows the reconstructed angle of attack and sideslip angle along the entire trajectory (left) and for Mach 3.0 conditions and below (right). As discussed above, during the hypersonic phase, the RV was unguided but spin-stabilized and began re-entry along a ballistic trajectory with the aeroshell in its zero-g inflation location. Until settled into its nominal drag position on the RV, the aeroshell orientation was sufficiently off-center to trim the RV to a maximum angle of attack of approximately -4.29° and sideslip angle of 5.90°. As expected, the RV attitude began to increase as the vehicle decelerated through supersonic to subsonic conditions due to the inherent dynamic instability of the shape. Even so, the maximum angles of attack and sideslip over the entire reconstructed trajectory were 9.12° and 9.39°, respectively, well below the 20° LOFTID mission requirement for stability. LOFTID was the first flight and opportunity to gather data on the stability and performance of a blunt body aeroshell geometry with no backshell through transonic and subsonic conditions, and on-board video data confirmed no attitude or attitude rate excursions.

The EDM jettison was triggered by timer and occurred 2260.0 s after RV separation. The EV altitude was 18.17 km, M_∞ = 0.29, and α_T = 4.36°. The timed trigger was set based on the longest possible time of flight within the launch window. LOFTID launched in the back third of the launch window, resulting in a shorter time of flight, and subsequently, the EDM deployed significantly later than the Mach 0.7 target condition. The vehicle attitude and attitude rates were well within expected limits, and the EDM successfully jettisoned and was later recovered from the Pacific Ocean by the recovery vessel.

The pilot chute deployed at Mach 0.11 (V_∞ = 35.21 m/s) and an altitude of 5.72 km, with α_T = 2.09°. Similar to the EDM, the pilot chute trigger was also set based on the longest possible time of flight for LOFTID, and the actual time of flight was considerably shorter. The main parachute deployment occurred shortly thereafter, at Mach 0.09 (V_∞ = 28.65 m/s) and an altitude of 5.59 km. The reconstructed spin rate estimate was 17.7 deg/s, with 18.0 deg/s being the nominal spin rate, and nearly zero rate in either minor axis.

The RV splashed down 3356.4 s after separating from the launch vehicle, 5.5346 nmi from the target. This splashdown position was close enough for the recovery vessel to visibly observe the descent of the RV under the parachute. The RV was observed from onboard the recovery vessel to be highly stable underneath the parachute. The RV was subsequently recovered from the ocean, and the inflatable structure fully retained its structural integrity.

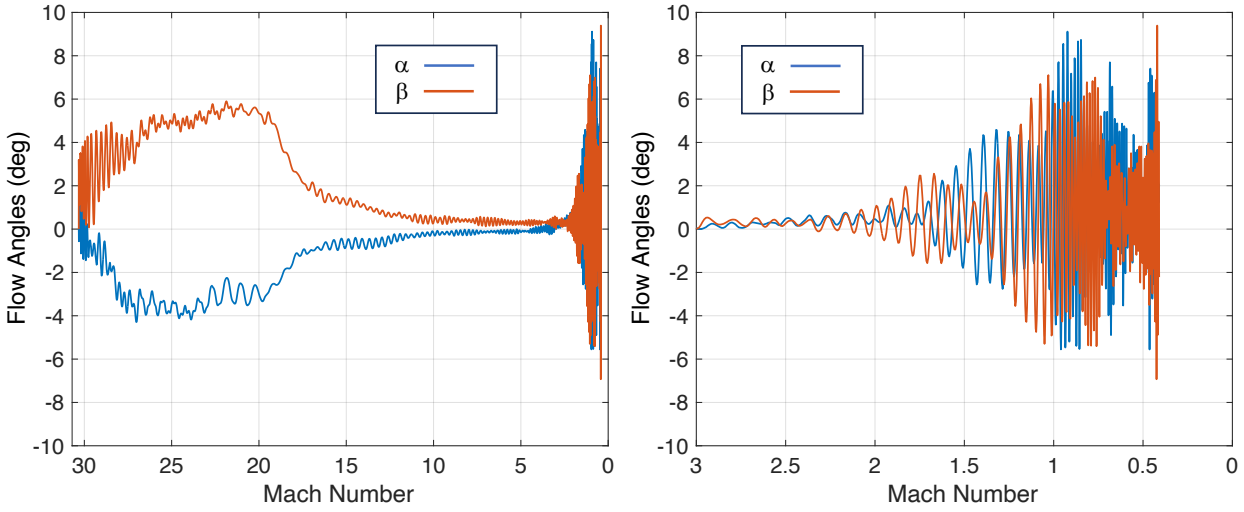

Fig. 11 Reconstructed Angle of Attack and Sideslip.

The LOFTID technology demonstration mission was fully successful in meeting both the stability and decelerator performance requirements.

IV. Conclusions

The LOFTID mission successfully demonstrated the deployment and entry performance of a 6 m diameter Hypersonic Inflatable Decelerator from low-earth orbit on November 10, 2022. The aerodynamics database for LOFTID leveraged and expanded on the flight experience from the suborbital IRVE and IRVE-3 missions and other planetary and Earth sample return missions. Both the re-entry vehicle and ejectable data module were successfully recovered from the Pacific Ocean, with LOFTID satisfying requirements for decelerator performance and stable flight from orbital entry conditions through parachute deployment and splashdown. LOFTID demonstrated inflatable aeroshell technology at scale and conditions relevant to multiple EDL applications, including Earth and Mars, further advancing the capability for low-mass, high performance decelerator systems.

Acknowledgments

The authors would like to acknowledge the support from the NASA Space Technology Mission Directorate's Technology Demonstration Mission Program and NASA's partnership with United Launch Alliance on this mission.

References

[1] DiNonno, J. C., and Cheatwood, F. M., "Low-Earth Orbit Flight Test of an Inflatable Decelerator (LOFTID) Mission Overview and Science Return," AIAA Paper 2024–XXXX, January 2024.

[2] Hughes, S. J., Dillman, R. A., Starr, B. R., Stephan, R. A., Lindell, M. C., Player, C. J., and Cheatwood, F. M., "Inflatable Reentry Vehicle Experiment (IRVE) Design Overview," AIAA Paper 2005–1636, May 2005.

[3] Olds, A. D., Beck, R. E., Bose, D. M., White, J. P., Edquist, K. T., Hollis, B. R., Lindell, M. C., Cheatwood, F. M., Gsell, V. T., and Bowden, E. L., "IRVE-3 Post-Flight Reconstruction," AIAA Paper 2013–1390, March 2013.

[4] Swanson, G. T., Kazemba, C. D., Miller, R. A., Alpert, H. S., Williams, J. D., Hughes, S. J., and Cheatwood, F. M., "Overview and Performance of the LOFTID Instrumentation Suite," AIAA Paper 2024–XXXX, January 2024.

[5] Karlgaard, C. D., Deshmukh, R. G., Dutta, S., Korzun, A. M., and Hollis, B. R., "Trajectory Reconstruction of the Low-Earth Orbit Flight Test of an Inflatable Decelerator," AIAA Paper 2024–XXXX, January 2024.

[6] Deshmukh, R. G., Dutta, S., Bowes, A., and DiNonno, J. C., "Flight Mechanics Analysis of Low-Earth Orbit Flight Test of an Inflatable Decelerator," AIAA Paper 2024–XXXX, January 2024.

[7] Moss, J. N., Glass, C. E., Hollis, B. R., and Norman, J. W. V., "Low-Density Aerodynamics for the Inflatable Reentry Vehicle Experiment," *Journal of Spacecraft and Rockets*, Vol. 43, No. 6, 2006, pp. 1191–1201.

[8] Schoenenberger, M., Cheatwood, F. M., and Desai, P. N., "Static Aerodynamics of the Mars Exploration Rover Entry Capsule," AIAA Paper 2005–0056, January 2005.

[9] Edquist, K. T., Desai, P. N., and Schoenenberger, M., "Aerodynamics for Mars Phoenix Entry Capsule," *Journal of Spacecraft and Rockets*, Vol. 48, No. 5, 2011, pp. 713–726.

[10] Schoenenberger, M., Norman, J. W. V., Karlgaard, C. D., Kutty, P., and Way, D. W., "Assessment of the Reconstructed Aerodynamics of the Mars Science Laboratory Entry Vehicle," *Journal of Spacecraft and Rockets*, Vol. 51, No. 4, 2014, pp. 1076–1093.

[11] Hollis, B. R., Wise, A. J., Liechty, D. S., and Korzun, A. M., "Aerothermodynamics Analyses for the LOFTID Technology Demonstration Mission," AIAA Paper 2024–XXXX, January 2024.

[12] Lebeau, G. J., and Lumkin, F. E., "Application Highlights of the DSMC Analysis Code (DAC) Software for Simulating Rarefied Flows," *Computer Methods in Applied Mechanics and Engineering*, Vol. 191, No. 6-7, 2001, pp. 595–609. https://doi.org/10.1016/S0045-7825(01)00304-8.

[13] Liechty, D. S., "Object-Oriented/Data-Oriented Design of a Direct Simulation Monte Carlo Algorithm," AIAA Paper 2014–2456, June 2014.

[14] Mazaheri, A., Gnoffo, P. A., Johnson, C. O., and Kleb, W. L., "LAURA User's Manual: 5.5-65135," NASA TM NASA TM-2013-217800, February 2011.

[15] Biedron, R. T., Carlson, J., Derlaga, J. M., Gnoffo, P. A., and et al., "FUN3D Manual: 13.5," NASA TM NASA TM-2019-220271, April 2019.

[16] Gnoffo, P. A., "An Upwind-Biased, Point-Implicit Algorithm for Viscous, Compressible Perfect-Gas Flows," NASA TP NASA TP-2953, February 1990.

[17] Korzun, A. M., Maddock, R. W., Schoenenberger, M., Edquist, K. T., Zumwalt, C. H., and Karlgaard, C. D., "Aerodynamic Performance of the InSight Mars Lander," *Journal of Spacecraft and Rockets*, Vol. 58, No. 5, 2021, pp. 1522–1529. https://doi.org/10.2514/1.A35085.

[18] Kazemba, C. D., Braun, R. D., Schoenenberger, M., and Clark, I. G., "Dynamic Stability Analysis of Blunt-Body Entry Vehicles Using Time-Lagged Aftbody Pitching Moments," *Journal of Spacecraft and Rockets*, Vol. 52, No. 2, 2015, pp. 393–403.